



Implementing a non-local means method to CTA data of aortic dissection

Maya Fitria^{1*}, Cosmin Adrian Morariu², Josef Pauli², Ramzi Adriman¹

¹Department of Computer and Electrical Engineering, Faculty of Engineering, Universitas Syiah Kuala
Jl. Tgk. Syech Abdur Rauf No. 7 Kopelma Darussalam, Banda Aceh, Indonesia 23111

²Department of Intelligent Systems, Faculty of Engineering, University of Duisburg-Essen
Bismarckstrasse 90, Building BC, 4. Floor, Duisburg, Germany 47057

How to cite: M. Fitria, C. A. Morariu, J. Pauli, and R. Adriman, "Implementing a non-local means method to CTA data of aortic dissection," *Jurnal Teknologi dan Sistem Komputer*, vol. 9, no. 3, pp. 174-179, 2021. doi: [10.14710/jtsiskom.2021.14125](https://doi.org/10.14710/jtsiskom.2021.14125), [Online].

Abstract – It is necessary to conserve important information, like edges, details, and textures, in CT aortic dissection images, as this helps the radiologist examine and diagnose the disease. Hence, a less noisy image is required to support medical experts in performing better diagnoses. In this work, the non-local means (NLM) method is conducted to minimize the noise in CT images of aortic dissection patients as a preprocessing step to produce accurate aortic segmentation results. The method is implemented in an existing segmentation system using six different kernel functions, and the evaluation is done by assessing DSC, precision, and recall of segmentation results. Furthermore, the visual quality of denoised images is also taken into account to be determined. Besides, a comparative analysis between NLM and other denoising methods is done in this experiment. The results showed that NLM yields encouraging segmentation results, even though the visualization of denoised images is unacceptable. Applying the NLM algorithm with the flat function provides the highest DSC, precision, and recall values of 0.937101, 0.954835, and 0.920517 consecutively.

Keywords - aortic dissection; noise reduction; non-local means, CT image, denoising method;

I. INTRODUCTION

It is a fact that some unwanted elements contaminate most images, so-called noise [1]. Noise can occur in images for many reasons [2]. It may appear as a consequence of the heat of the image sensors, and it also may arise during the image is taken or transmission of the image itself [3]. Biomedical images produced by some imaging techniques, such as CT scanning, indeed contain some visual noise. The appearance of noise restricts the radiologist's performance to differentiate inhomogeneous regions in the image [4]. This noise may lead to uncertainty in interpreting the image and degrade diagnostic performance [5]. Thus, the main purpose of this work concerns removing or at least

reducing noise shown in CT scan images of aortic dissection patients. The aim of the noise reduction process itself is to improve the aortic boundary detection phase of 3D aortic segmentation and to reconstruct the 3D surface of the aorta, as discussed in [6]-[8]. Hence, removing noise in the MPR image is mandatory to increase aorta localization's whole performance. In [9], some denoising techniques, such as Gaussian filter, anisotropic diffusion, Yaroslavsky filter, and bilateral filter, are implemented in the system. The segmentation results obtained are quite encouraging. However, the visual images constructed are unsatisfied, where the blurry effect happened, and grainy parts are over smoothed.

In recent years, non-local means filter (NLM) has attracted significant attention among other techniques. Many studies, such as in [10]-[15], adapted the NLM methods to process noisy images and proved that NLM yields outperforming results. Non-local means (NLM) is a noise reduction technique proposed by Buades et al. [16]-[18]. This technique is inspired by neighborhood filtering, which removes noise based on local averaging [19]. However, in the NLM method, all pixel values in the image take part in the non-local smoothing process. The idea of this algorithm is taken from the fact that every patch in any raw image has many other similar patches [16]. These similarity patches will be taken into account for removing the noise. This method aims to replace the intensity values in each pixel with the weighted average of other similar patches in the full image.

In the NLM method, a kernel function acts as the degree of filtering to compute weighting factors of search neighborhood pixels [20]. This function delineated the similarity between patches and is in charge of weighting factor measurement. There are six kernel functions proposed in NLM. The first function is introduced by Buades et al. [16], namely the exponential function. Tian et al. [21] proposed other kernel functions, namely cosine function, flat function, Gaussian function, turkey bi-weight function, and wave function.

This work aims to continue the work that has been done in [9] by embedding another denoising method, i.e., NLM, to CTA data of aortic dissection. This filter

*Correspondence author (Maya Fitria)
Email: mayafitria@unsyiah.ac.id

can exploit the inherent redundant information and preserve high degree image texture and details in CT scan images [5]. The classic NLM method is installed and established with six different kernel functions in this experiment. Furthermore, the comparison result between other denoising techniques will be done in the experiment.

II. RESEARCH METHODS

NLM method was implemented in the aortic segmentation system discussed in [6]-[8]. The segmentation process is divided into five steps (see Figure 1). Initialization places at least three points inside the aorta to obtain an approximation of the aortic centerline. Multiplanar Reformat (MPR) Images Extraction uses an aortic centerline to generate images in the two-dimensional region of interest with size $m \times m$. The MPR images are stored in the MPR stack. Aorta Localization aims to detect aortic circles in extracted MPR images. Contour deformation is done by adjusting the detected circle in the MPR image to meet the shape of the aortic contour. The 3D model construction is based on segmented results reformed in contour deformation step.

The method mainly runs in the preprocessing phase of the aortic localization step, where extracted grayscale MPR images are iteratively being used, denoised, and circle candidates are placed onto it. The optimal circles are selected in the post-processing phase and visualized in a 3D plot. The original images whose noises will be removed are taken from the stack and in the form of grayscale MPR images. The procedure of the denoising process is illustrated in Figure 2. Every image in the MPR stack will be denoised using NLM established with different kernel functions, namely exponential function, cosine function, flat function, Gaussian function, turkey bi-weight function, and wave function. The kernel functions are successively expressed in (1)–(6) [16], [21]. Basically, for a pixel x which is considered for denoising, NLM will search in the full image to find other patches which look alike the reference patches whose centre pixel is x . λ in the equations plays the role of a parameter to control the quality of filtering. The graphical representation of the six kernel functions can be seen in Figure 3.

$$f(x) = e^{-\frac{x}{\lambda}} \quad (1)$$

$$f(x) = \begin{cases} \cos\left(\frac{\pi x}{2\lambda}\right) & ; 0 < x \leq \lambda \\ 0 & ; else \end{cases} \quad (2)$$

$$f(x) = \begin{cases} \frac{1}{x} & ; 0 < x \leq \lambda \\ 0 & ; else \end{cases} \quad (3)$$

$$f(x) = e^{\left(\frac{-x^2}{2\lambda^2}\right)} ; x > 0 \quad (4)$$

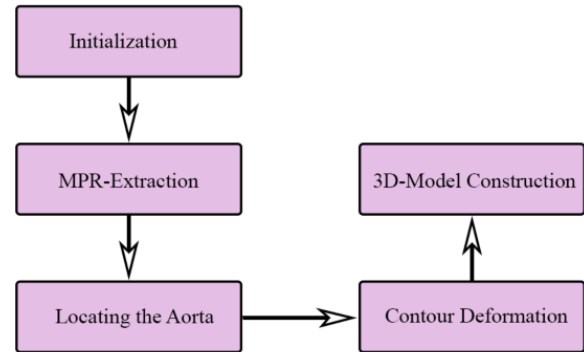


Figure 1. Steps of existing aorta segmentation system

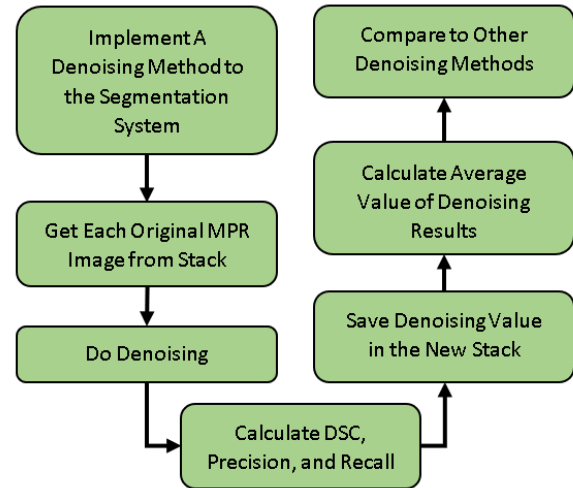


Figure 2. Research procedure [9]

$$f(x) = \begin{cases} \frac{1}{2} \left(1 - \left(\frac{x}{\lambda}\right)^2\right)^2 & ; 0 < x \leq \lambda \\ 0 & ; else \end{cases} \quad (5)$$

$$f(x) = \begin{cases} \frac{\pi x}{\pi x \lambda} & ; 0 < x \leq \lambda \\ 0 & ; else \end{cases} \quad (6)$$

After the denoising process, the segmentation result of each MPR will be calculated and saved in a new stack. The average segmentation value of whole MPR images will be measured. Furthermore, the comparison result between other denoising techniques will be done in the experiment.

A. Dataset and method implementation

This work uses Computed Tomography Angiography (CTA) images of patients with aortic dissection cases provided by West German Heart Center of Essen-University Hospital. The number of datasets used for examination is 11 datasets sliced between 89–1034 slices with a 0.7–5 mm slice gap, and each axial slice has a resolution range between 0.445 to 0.863 mm [9].

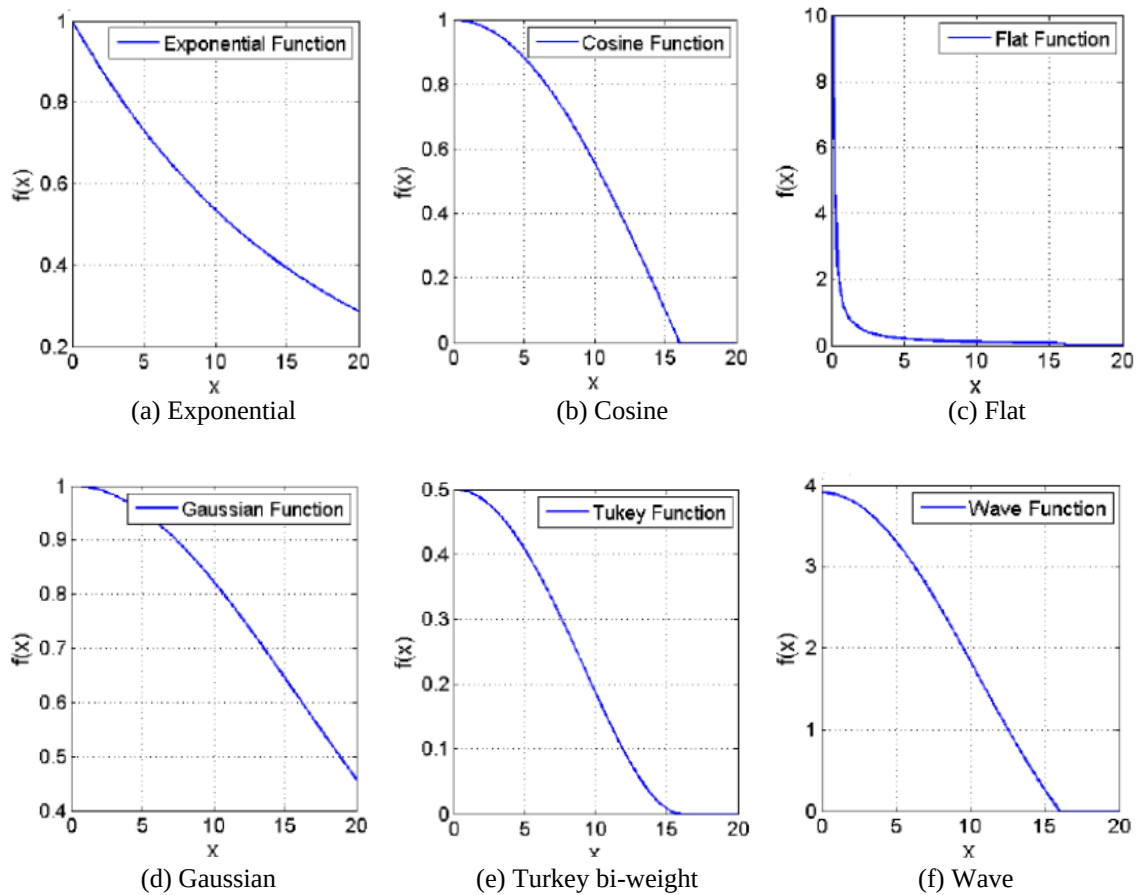


Figure 3. Various kernel functions with a particular parameter λ [21]

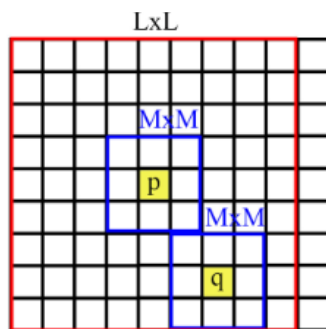


Figure 4. Illustration of the patch-based methodology of NLM method

The implementation of NLM methods in this experiment adopted the source from [21]. Figure 4 depicts how an $m \times m$ region centered at pixel q searches other similar regions of the same size in a search region of the full image, for example, in the patch centered at pixel p . The search region can also be set in the $L \times L$ neighborhood region centered at pixel p . Thus, several parameters have to be settled before denoising. The parameter sets are exhibited in Table 1. Due to the large number of MPR images provided for each CTA dataset, the selection of parameter M is set to be small to prevent a time-consuming evaluation. Like M , the size of search window L in this experiment has to be restricted to a small value.

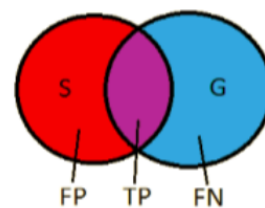


Figure 5. How aorta ground truth and segmentation result after denoising being compared [9]

Table 1. Parameter set of NLM Method

No	Parameter	Value
1.	M	5
2.	L	15
3.	λ	200

B. Evaluation model

In this study, the manually segmented images of CTA scans are used as ground truth images. Figure 5 depicts the comparison of aorta ground truth and segmentation output after denoising that leads into four combinations of comparison results, namely True Positive (TP), True Negative (TN), False Positive (FP), and False Negative (FN). TP is when the voxel in the G and S. TN is when the voxel belongs to the background

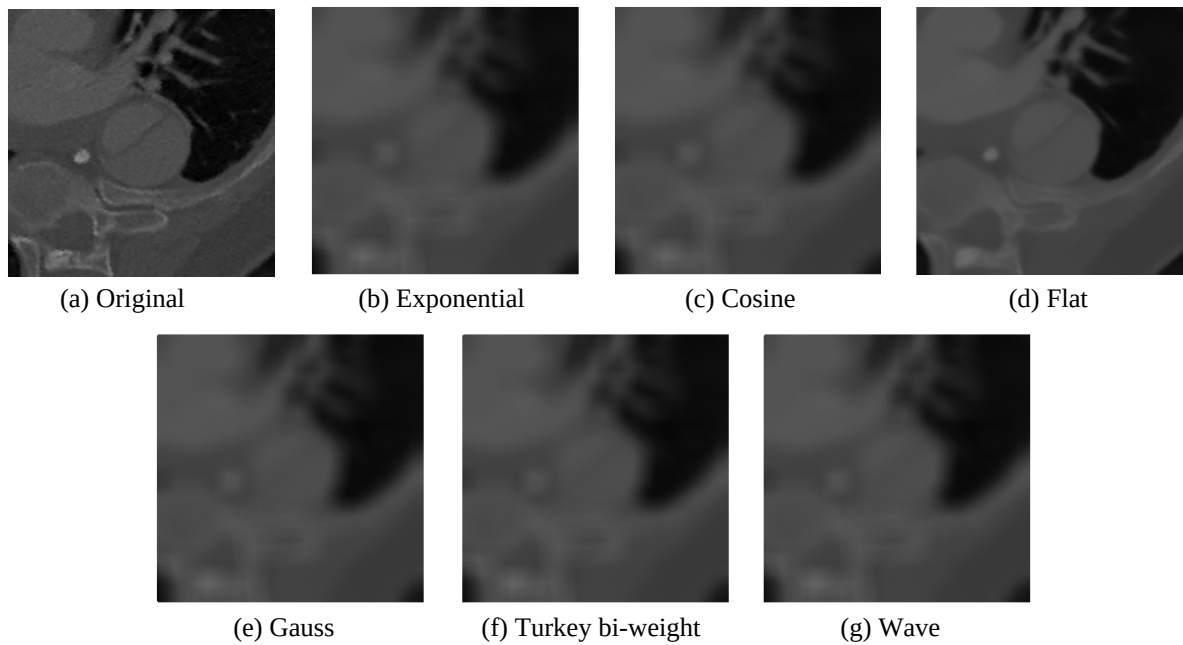


Figure 6. Image comparison between original image and NLM denoised image established with different kernels

of G and S. FP is when the voxel in the S and the background of G. FN is when the voxel in the G and the background of S.

The method performance is examined by analyzing the quality of output images. However, it is not enough to judge restored images using only one criterion since judging quality images could vary from person to person. Thus, to assess the output of NLM implemented in the systems, the evaluation model is divided into qualitative and quantitative assessments. Qualitative assessment is done by analyzing the quality of the output image. On the other hand, the quantitative model uses the measurement of dice similarity coefficient (DSC), precision (P), and recall (R) based on four combinations above by using (7)-(9). The DSC will give values between 0 to 1. The higher the DSC, the better the result.

$$P = \frac{TP}{TP + FP} \quad (7)$$

$$R = \frac{TP}{TP + FN} \quad (8)$$

$$DSC = \frac{2 \times P \times R}{P + R} \quad (9)$$

III. RESULTS AND DISCUSSION

Denoised images of the NLM method applied in this work are visualized in Figure 6. Figure 6(d) shows that visual performance NLM with flat function preserves the flat objects and the edges.. Different from the flat function, using the other kernel functions return blurry images. The visual results are contrary to the results that have been proven in [8] and [9], where the NLM algorithm shows outstanding visual performance. The

Table 2. Segmentation results of exponential function

Patients	DSC	Precision	Recall
1	0.926291	0.967930	0.888087
2	0.932901	0.979531	0.890508
3	0.929526	0.917587	0.941779
4	0.925930	0.911840	0.940462
5	0.928975	0.908452	0.950448
6	0.843585	0.824224	0.863879
7	0.906572	0.932722	0.881848
8	0.944519	0.935925	0.953273
9	0.920613	0.944716	0.897708
10	0.894083	0.954697	0.840706
11	0.898248	0.923865	0.874013
Average	0.913749	0.927408	0.902064
Standar deviation	0.027836	0.041062	0.038446

poor-quality performance of NLM occurs because of resolution range in MPR images extracted by the system is too small, which is in the range of 0 to 1. The size of the pixel value in the image affected the computation of the kernel function. The smaller the intensity values, the smaller the kernel function itself.

Table 2 illustrates the segmentation results of NLM established with an exponential kernel. There are some datasets (patient 10 and 11) that produce DSC values below 0,9. Nevertheless, it remains good in the average with DSC 0.913479, precision 0.927408, and recall 0.902064. Compared to the exponential kernel, employing flat function in NLM method yields a slightly increasing result of average DSC 0.937101, precision 0.954835, and recall 0.920517, as seen in Table 3. This result confirms the results presented by Tian et al. [21] that the application of NLM using a flat

Table 3. Segmentation results of flat function

Patients	DSC	Precision	Recall
1	0.931448	0.981117	0.886566
2	0.934189	0.976087	0.895740
3	0.938398	0.938436	0.938360
4	0.946095	0.947885	0.944311
5	0.921018	0.943625	0.894609
6	0.940825	0.931154	0.911100
7	0.940825	0.949125	0.932668
8	0.959652	0.958392	0.960914
9	0.947721	0.957759	0.937892
10	0.926960	0.947115	0.907646
11	0.943345	0.972499	0.915888
Average	0.937101	0.954835	0.920517
Standard deviation	0.012272	0.016035	0.023831

kernel outperforms the result of NLM with the exponential kernel.

Despite the other kernel function, specifically cosine function, Gaussian function, Turkey bi-weight function, and wave function, yields poor-quality image, fascinating segmentation results appear during NLM experiment configured with those kernels. Applying those four kernels returns exactly the same segmentation result value (DSC, precision, and recall). These values are shown in [Table 4](#).

The same segmentation results are caused by the shape of these functions that are roughly resemblant (see [Figure 3](#)). Moreover, selecting a small mask M as a parameter emerges as another factor of similar segmentation results. However, the outcome is quite satisfying, with an average DSC of 0.913711. The value is also similar to the value of the exponential function.

Another criterion to be assessed in this study is by comparing NLM segmentation results with the results after applying other denoising techniques in [\[9\]](#). [Table 5](#) summarizes the average value of segmentation performances between NLM with six kernel functions, Gaussian filter, anisotropic diffusion, Yaroslavsky filter, and bilateral filter. Identified by the table, applying the NLM algorithm with flat function provides the highest value of DSC, 0.937101. The bilateral filter occupies the second-highest rank among the other algorithms, with a

Table 4. Segmentation results obtained by establishing cosine function, Gaussian function, turkey bi-weight function, and wave function

Patients	DSC	Precision	Recall
1	0.926483	0.967976	0.888401
2	0.932740	0.980165	0.889692
3	0.929652	0.917570	0.942057
4	0.925908	0.911799	0.940460
5	0.928975	0.908452	0.950448
6	0.842856	0.822844	0.822844
7	0.906430	0.932854	0.932854
8	0.944538	0.935958	0.953275
9	0.920623	0.944683	0.897758
10	0.894122	0.954691	0.840780
11	0.898497	0.923199	0.875082
Average	0.913711	0.927290	0.911284
Standard deviation	0.028014	0.041503	0.036219

DSC value of 0.936310. Surprisingly, the Gaussian filter, commonly known as the blurring technique, also provides almost similar value to the first and second highest results. On the other hand, establishing the other five kernels in NLM reduces the performance of segmentation results. They hold the worst segmentation performance among the others.

IV. CONCLUSION

Employing NLM kernel functions as denoising process obtains overall outstanding segmentation results and is suitable to be used to get satisfying DSC values, in point of fact by using flat kernel function with highest DSC among them. Nonetheless, blurry images occur after applying all kernel functions, except using the flat function. This occurrence arises due to the small pixel range in the CTA image and influences the weighting factor measurement. In future work, the intensity value of images must be considered to obtain better-filtered images of the NLM algorithm. In addition, another aspect regarding efficiency should be investigated in the future since the computational speed of NLM is insufficient to be used in the system.

Table 5. Comparison of denoising methods in [\[9\]](#) and NLM with different kernel functions

Denoising Technique	DSC	Precision	Recall
Gaussian filter	0.936196	0.956233	0.917386
Anisotropic diffusion	0.931688	0.960567	0.904948
Yaroslavsky filter	0.928737	0.941651	0.917904
Bilateral filter	0.936310	0.955957	0.918054
NLM exponential function	0.913749	0.927408	0.902064
NLM cosine function	0.913711	0.927290	0.911284
NLM flat function	0.937101	0.954835	0.920517
NLM gauss function	0.913711	0.928070	0.911284
NLM turkey function	0.913711	0.928070	0.911284
NLM wave function	0.913711	0.928070	0.911284

REFERENCES

- [1] K. S. Sankaran and N. V. Nagappan, "Noise free image restoration using hybrid filter with adaptive genetic algorithm," *Computers and Electrical Engineering*, vol. 54, pp. 382-392, 2016. doi: [10.1016/j.compeleceng.2015.12.011](https://doi.org/10.1016/j.compeleceng.2015.12.011)
- [2] C. Bonchelet, "Image noise models," in *The Essential Guide to Image Processing*, 2nd ed. Academic Press, 2009, pp. 143-167. doi: [10.1016/B978-0-12-374457-9.00007-X](https://doi.org/10.1016/B978-0-12-374457-9.00007-X)
- [3] A. M. Hambal, Z. Pei, and F. L. Ishabailu, "Image noise reduction and filtering techniques," *International Journal of Science and Research*, vol. 6, no. 3, pp. 2033-2038, 2017.
- [4] S. E. Darmanayagam, K. N. Harichandran, S. R. R. Cyril, and K. Arputharaj, K, "A novel supervised approach for segmentation of lung parenchyma from chest CT for computer-aided diagnosis," *Journal of Digital Imaging*, vol. 26, no. 3, pp. 496-509, 2013. doi: [10.1007/s10278-012-9539-6](https://doi.org/10.1007/s10278-012-9539-6)
- [5] Z. Li, L. Yu, J. D. Trzasko, D. S. Lake, D. J. Blezek, J. G. Fletcher, C. H. McCollough, and A. Manduca, "Adaptive nonlocal means filtering based on local noise level for CT denoising," *Medical Physics*, vol. 41, no. 1, 011908, 2014. doi: [10.1118/1.4851635](https://doi.org/10.1118/1.4851635)
- [6] C. A. Morariu, D. S. Dohle, T. Terheiden, K. Tsagakis, and J. Pauli, "Polar-based aortic segmentation in 3D CTA dissection data using a piecewise constant curvature model," in *Informatik aktuell*. Berlin: Springer, 2014, pp. 390-395. doi: [10.1007/978-3-642-54111-7_71](https://doi.org/10.1007/978-3-642-54111-7_71)
- [7] C. A. Morariu, T. Terheiden, D.S. Dohle, K. Tsagakis, and J. Pauli, "Graph-based and variational minimization of statistical cost functionals for 3d segmentation of aortic dissections," in *German Conference on Pattern Recognition*, Munster, Germany, Sep. 2014, pp. 511-522. doi: [10.1007/978-3-319-11752-2_42](https://doi.org/10.1007/978-3-319-11752-2_42)
- [8] C. A. Morariu, T. Terheiden, D.S. Dohle, K. Tsagakis, and J. Pauli, "Increasing the feasibility of minimally invasive procedures in type A aortic dissections: a framework for segmentation and quantification," *International Journal of Computer Assisted Radiology and Surgery*, vol. 11, no. 2, pp. 243-252, 2016. doi: [10.1007/s11548-015-1283-1](https://doi.org/10.1007/s11548-015-1283-1)
- [9] M. Fitria, R. Adriman, C. A. Morariu, and J. Pauli, "Comparison of denoising methods applied to CTA Images of 3D segmentation of aortic dissection," in *IEEE International Conference on Cybernetics and Computational Intelligence*, Banda Aceh, Indonesia, Aug. 2019, pp. 92-97. doi: [10.1109/CYBERNETICSCOM.2019.8875635](https://doi.org/10.1109/CYBERNETICSCOM.2019.8875635)
- [10] Y. Wu, B. Tracey, P. Natarajan, and J. P. Noonan, "James-stein type center pixel weights for non-local means image denoising," *IEEE Signal Processing Letters*, vol. 20, no. 4, pp. 411-414, 2013. doi: [10.1109/LSP.2013.2247755](https://doi.org/10.1109/LSP.2013.2247755)
- [11] Y. Chen, Z. Yang, Y. Hu, G. Yang, Y. Zhu, Y. Li, L. Luo, W. Chen, and C. Toumoulin, "Thoracic low-dose CT image processing using an artifact suppressed large-scale nonlocal means," *Physics in Medicine and Biology*, vol. 57, no. 9, 2667, 2012. doi: [10.1088/0031-9155/57/9/2667](https://doi.org/10.1088/0031-9155/57/9/2667)
- [12] L. Lu, W. Jin, and X. Wang, "Non-local means image denoising with a soft threshold," *IEEE Signal Processing Letters*, vol. 22, no. 7, pp. 833-837, 2015. doi: [10.1109/LSP.2014.2371332](https://doi.org/10.1109/LSP.2014.2371332)
- [13] H. Zhang, D. Zeng, H. Zhang, J. Wang, Z. Liang, and J. Ma, "Applications of nonlocal means algorithm in low-dose X-ray CT image processing and reconstruction: A review," *Medical Physics*, vol. 44, no. 3, pp. 1168-1185, 2017. doi: [10.1002/mp.12097](https://doi.org/10.1002/mp.12097)
- [14] V. Fedorov, and C. Ballester, "Affine non-local means image denoising," *IEEE Transactions on Image Processing*, vol. 26, no. 5, pp. 2137-2148, 2017. doi: [10.1109/TIP.2017.2681421](https://doi.org/10.1109/TIP.2017.2681421)
- [15] P. Nair, and K. N. Chaudhury, "Fast high-dimensional bilateral and nonlocal means filtering," *IEEE Transactions on Image Processing*, vol. 28, no. 3, pp. 1470-1481, 2019. doi: [10.1109/TIP.2018.2878955](https://doi.org/10.1109/TIP.2018.2878955)
- [16] A. Buades, B. Coll, and J. M. Morel, "A non-local algorithm for image denoising," in *IEEE Computer Society Conference on Computer Vision and Pattern Recognition*, San Diego, USA, Jun. 2015, pp. 60-65. doi: [10.1109/CVPR.2005.38](https://doi.org/10.1109/CVPR.2005.38)
- [17] A. Buades, B. Coll, and J. M. Morel, "Nonlocal image and movie denoising," *International Journal of Computer Vision*, vol. 76, no. 2, pp 123-139, 2008. doi: [10.1007/s11263-007-0052-1](https://doi.org/10.1007/s11263-007-0052-1)
- [18] A. Buades, B. Coll, and J. M. Morel, "Image denoising methods. A new nonlocal principle," *SIAM Review*, vol. 52, no. 1, pp. 113-147, 2010. doi: [10.1137/090773908](https://doi.org/10.1137/090773908)
- [19] J. M. Morel, A. Buades, and T. Coll, "Local smoothing neighborhood filters," in *Handbook of Mathematical Methods in Imaging*, 2nd ed. New York: Springer, 2015, pp. 1599-1643. doi: [10.1007/978-1-4939-0790-8_26](https://doi.org/10.1007/978-1-4939-0790-8_26)
- [20] Z. M. Ramadan, "An innovative kernel function for the NLM filtering," *ARNP Journal of Engineering and Applied Science*, vol. 15, no. 7, 2020.
- [21] J. Tian, W. Y. Yu, and S. L. Xie, "On the kernel function selection of nonlocal filtering for image denoising," in *International Conference on Machine Learning and Cybernetics*, Kunming, China, Jul. 2008, pp. 2964-2969, 2008. doi: [10.1109/ICMLC.2008.4620915](https://doi.org/10.1109/ICMLC.2008.4620915)



©2021. This open-access article is distributed under the terms and conditions of the [Creative Commons Attribution-ShareAlike 4.0 International License](https://creativecommons.org/licenses/by-sa/4.0/).